Deep convolutional neural network denoising for digital breast tomosynthesis reconstruction

Gao, Mingjie, Samala, Ravi, Fessler, Jeffrey, Chan, Heang-Ping

Mingjie Gao, Ravi K. Samala, Jeffrey A. Fessler, Heang-Ping Chan, "Deep convolutional neural network denoising for digital breast tomosynthesis reconstruction," Proc. SPIE 11312, Medical Imaging 2020: Physics of Medical Imaging, 113120Q (16 March 2020); doi: 10.1117/12.2549361

SPIE.

Event: SPIE Medical Imaging, 2020, Houston, Texas, United States

Deep Convolutional Neural Network Denoising for Digital Breast Tomosynthesis Reconstruction

Mingjie Gao*[a,b], Ravi K. Samala[a], Jeffrey A. Fessler[a,b], Heang-Ping Chan**[a]

[a]Department of Radiology, University of Michigan, Ann Arbor, MI 48109;
[b]Department of Electrical Engineering and Computer Science, University of Michigan, Ann Arbor, MI 48109

Abstract

To reduce noise and enhance the contrast-to-noise ratio (CNR) of microcalcifications (MCs) in digital breast tomosynthesis (DBT), we conducted a study to investigate the feasibility of performing denoising on the projection views (PVs) using a deep convolutional neural network (DCNN) before reconstruction. We fine-tuned a modularized adaptive processing neural network (MAPNN) based on a pretrained model for CT image denoising. Four phantom DBTs containing over 700 simulated MCs of 3 nominal sizes were scanned with a DBT system that acquired 9 PVs within a 25° scan angle at two dose level settings to form the training and validation sets. Nine human subject DBTs were used as an independent test set. We trained the DCNN with low dose PVs as the input and the corresponding high dose PVs as the reference. We marked the MCs in the PVs and designed a loss function for DCNN training that balanced the effect of noise reduction and signal preservation. The loss function was a weighted sum of the perceptual loss, the adversarial loss and the CNR loss. A visual comparison of the DBT volumes reconstructed from the denoised PVs indicated that the proposed method could reduce noise and preserve the texture of the background without blurring subtle MC signals. A quantitative comparison showed a significant CNR improvement ($p < 0.0001$) in both the validation phantom and the human subject DBTs.

Keywords: digital breast tomosynthesis, image denoising, deep learning, microcalcification

1. INTRODUCTION

Digital breast tomosynthesis (DBT) has been designed to alleviate the problem of overlapping tissues in conventional mammography. A DBT scan acquires a small number of projection views (PVs) over a limited scan angle. A quasi-3D image is obtained from the 2D PVs using tomographic reconstruction. In DBT, each PV is much noisier than mammography because the total dose level of DBT is kept comparable to that of a single 2D mammogram. Therefore, it is important to control the noise level in DBT reconstruction. Our group has modeled the noise correlation caused by detector blur for iterative reconstruction of DBT [1].

In this study, we investigated the potential of a deep convolutional neural network (DCNN) in DBT denoising with focus on improving the conspicuity of microcalcifications (MCs). We examined the feasibility of performing PV denoising with a DCNN before DBT reconstruction. PVs in DBT are simply low-dose mammograms. However, as the signal-to-noise ratio of MCs in the PVs is much lower than that in the full dose mammograms, it is challenging to denoise the PVs and to preserve the MC signals at the same time. A previous study demonstrates that a neural network convolution (NNC) model with one convolutional layer could denoise low dose DBT images [2]. DCNN has found success in image processing areas such as image super-resolution and image denoising, and in particular, CT image denoising [3]–[5]. We adapted the modularized adaptive processing neural network (MAPNN) [5] to DBT denoising by designing a loss function based on the characteristics of the target task and fine-tuned the DCNN with DBT images of breast phantoms acquired at two different dose levels. We evaluated the proposed method using DBTs from both phantoms and human subjects.

Corresponding authors: *gmingjie@umich.edu; **chanhp@umich.edu

Medical Imaging 2020: Physics of Medical Imaging, edited by Guang-Hong Chen, Hilde Bosmans, Proc. of SPIE
Vol. 11312, 113120Q · © 2020 SPIE · CCC code: 1605-7422/20/$21 · doi: 10.1117/12.2549361

2. MATERIALS AND METHODS

2.1 Data set

We used six 1-cm-thick heterogeneous slabs with 50% glandular/50% adipose breast-tissue-equivalent material to construct the phantoms [6]. Four different 5-cm-thick phantoms were formed by arranging five of the six slabs in different orders and orientations. Clusters of simulated calcifications (glass beads) of three nominal sizes (subtle: 0.180-0.212 mm; medium: 0.212-0.250 mm; obvious: 0.250-0.300 mm) were randomly sandwiched between the slabs. The phantoms were scanned with a commercial DBT system (Pristina, GE Healthcare) that acquires 9 projections in an angular range of 25° with a CsI/Si flat panel detector of 0.1 mm×0.1 mm pixel pitch. Each phantom was imaged at two dose level settings (low dose: Rh/Ag 34 kVp, 34 mAs; high dose: Rh/Ag 34 kVp, 71 mAs) under the same compression. We marked the MCs in the reconstructed volumes, projected the MC locations to the PV domain using the DBT system geometry, and extracted a 32×32-pixel patch centered at each MC from each of the PVs. The gray level intensity of the PVs was scaled to account for the dose levels and log-transformed before patch extraction. The training set contained 5022 pairs of low dose/high dose patches from the PVs of three phantoms, corresponding to 198 subtle, 204 medium and 156 obvious MCs in the reconstructed volumes. The remaining phantom images containing 84 subtle, 70 medium and 53 obvious MCs in the volume were used for validation.

An independent test set contained nine DBT scans of human subjects acquired with a prototype DBT system (GEN2, GE Global Research). The prototype system acquires 21 PVs in a scan angle of 60°. We used the central 9 PVs that correspond to a scan angle of 24° and a 43% dose of the original scan to simulate a low dose DBT with scan parameters like a commercial DBT system. 301 MCs were marked in the reconstructed volumes.

2.2 DCNN denoiser

The DCNN architecture used in this study was the MAPNN that was proposed for CT image denoising [5]. The MAPNN sequentially applied a series of identical denoising modules to each image patch for progressive denoising. Compared with one-step denoising, progressive denoising was reported to achieve similar output noise level while preserving more of the subtle structures. The degree of smoothing can be controlled by selecting the number of denoising modules applied to the image.

Because MCs are important signals for breast cancer detection yet denoisers designed for CT images could not preserve the subtle MCs, we modified the DCNN training loss function for our application of PV denoising in DBT. Our loss function was composed of the perceptual loss, the adversarial loss and the contrast-to-noise ratio (CNR) loss:

$$L = L_{\text{Perceptual}} + \lambda_1 L_{\text{WGAN}} + \lambda_2 L_{\text{CNR}}, \quad (1)$$

where λ_1, λ_2 are the weighting parameters.

The perceptual loss $L_{\text{Perceptual}}$ compares high-level features instead of pixel-wise difference between two images [7]. We used the mean-squared error between the deep features extracted by a pretrained VGG16 network [8] from the DCNN processed low dose image and the reference image as the perceptual loss. The adversarial loss L_{WGAN} encourages the denoised low dose images and the reference images to have the same distribution. We used the Wasserstein Generative Adversarial Network (WGAN) with gradient penalty as the adversarial loss [9]. Note that the adversarial loss requires another network, the discriminator, to be trained with the DCNN denoiser at the same time. We designed the CNR loss L_{CNR} to guide the denoiser to preserve the signal while smoothing the noise. The CNR is defined as the maximum of the MC signal divided by the noise standard deviation in the patch after background removal, as illustrated in Figure 1. We used the mean-squared difference of the CNR values as the CNR loss.

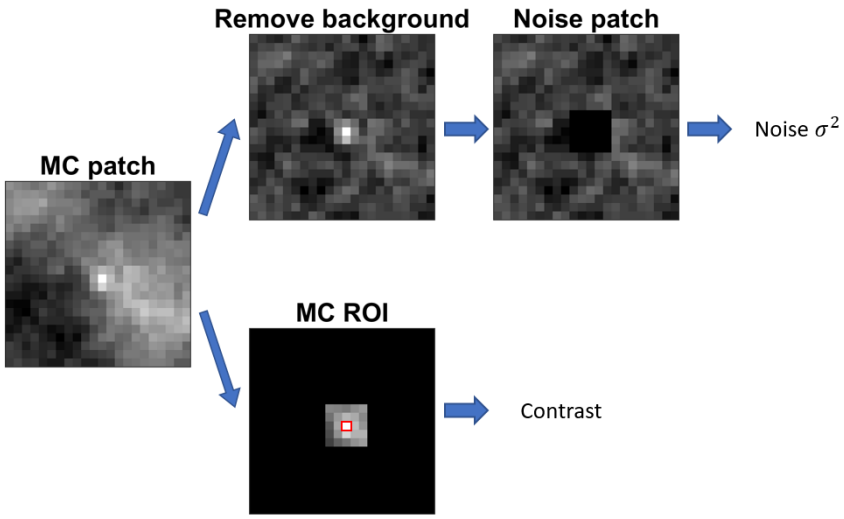

Figure 1. An illustration of CNR calculation for the CNR loss. For the noise calculation, we first apply a band pass filter [10] to remove background, and then calculate the standard deviation value of the noise patch. We take the maximum voxel values of the MC as the signal contrast.

2.3 Figure of merit

To quantitatively evaluate the effect of PV denoising for DBT reconstruction, we calculated the CNR of each MC in the reconstructed volumes as a figure-of-merit. We obtained the contrast of an MC from the peak value of a Gaussian function fitted to the MC pixels. The background noise was estimated as the root-mean-squared noise in the surrounding area after removing the background and excluding the MC pixels. The use of the CNR for comparison directly evaluated the effect of denoising on the individual MCs without the influence of additional variables such as those in a computer-aided detection algorithm or those in a model observer.

We used the simultaneous algebraic reconstruction technique (SART) with the segmented separable footprint projector [11] to reconstruct DBT volumes using both the original PVs and the denoised PVs. The voxel size was 0.1 mm×0.1 mm×1 mm. We compared the calculated CNRs of an MC on its focal plane with and without denoising by the DCNN.

3. RESULTS

We experimentally found that using two denoising modules provided the best trade-off between noise smoothing and preserving the MC signals for the PVs of DBT. We also found that the pretrained DCNN denoiser for CT images without fine-tuning by our proposed method smoothed the PVs but also reduced the CNRs of the MCs. Because of the limited size of the training set, we fine-tuned the CNN model based on the pretrained model from [5]. Figure 2 shows the MC clusters of different sizes in the validation phantom reconstructed from the low dose, the fine-tuned DCNN denoised, and the high dose PVs. Compared to the low dose DBT, the denoised images are smoother so that the MCs were more conspicuous but were still not as high as those in the high dose DBT. Importantly, the MCs were not blurred, and the background texture was preserved after denoising and was comparable to the texture in the high dose images, which was often a challenge for other denoising techniques.

Figure 3 shows quantitative comparisons of the CNRs in the reconstructed DBT slices, specifically the CNR scatter plots of the denoised MCs vs. the low dose MCs for the three MC sizes in the validation phantom. The CNR values of subtle, medium and obvious MCs were improved by an average of 6.7%, 9.7% and 9.5%, respectively. Although the subtle MCs were small, most of the subtle MCs were enhanced after denoising, as can be seen by the data points above the diagonal

line. The CNRs of the medium and obvious MCs were improved more consistently compared to the subtle MCs. The improvement was statistically significant ($p < 0.0001$) with two-tailed paired t-test for all three sizes.

Figure 4 shows the CNR scatter plot of MCs from the human subject DBTs. The least squares fitting line is above the 10% gain reference line. Only a few MCs had lower CNRs after denoising. The improvement was statistically significant ($p < 0.0001$).

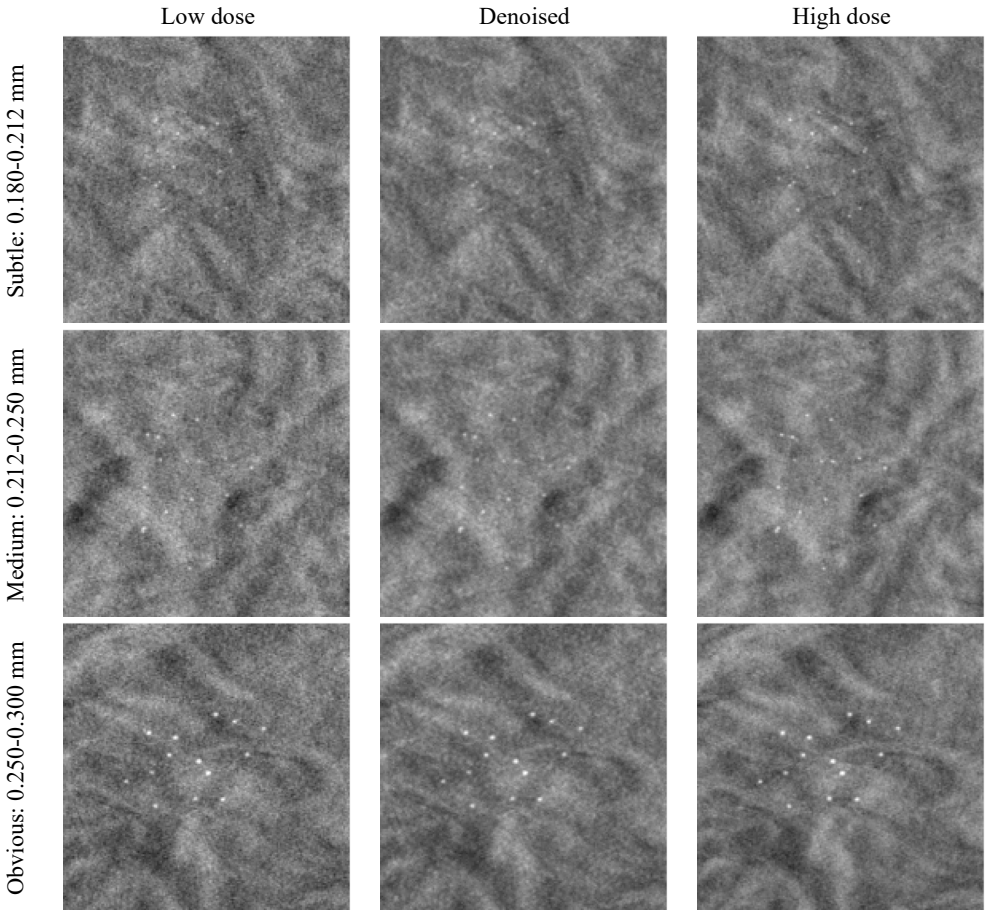

Figure 2. Three MC clusters of different sizes in the validation phantom volume reconstructed from different PVs. All images show an 18 mm×18 mm region in the original image and are displayed with the same window/level settings.

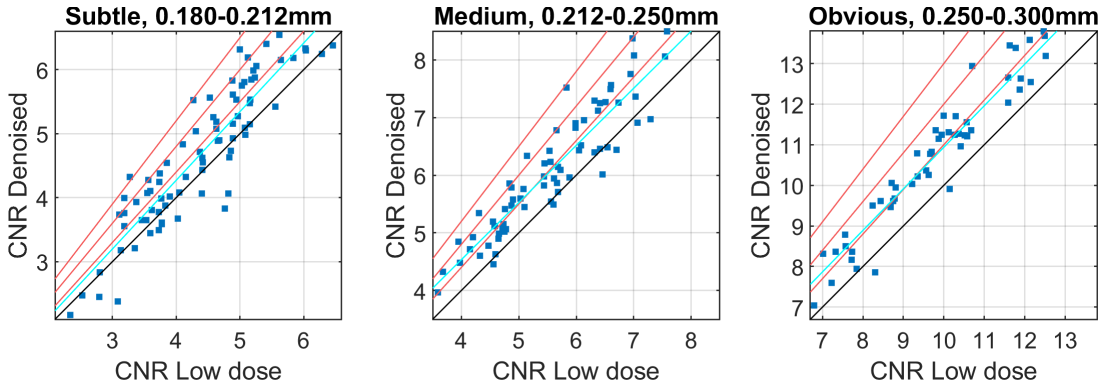

Figure 3. The CNR scatter plots of the denoised MCs vs. the low dose MCs for different MC sizes in the validation phantom volume. The cyan line indicates least squares fitting. The black line is the diagonal line. The red lines are reference lines indicating 10%, 20% and 30% gain.

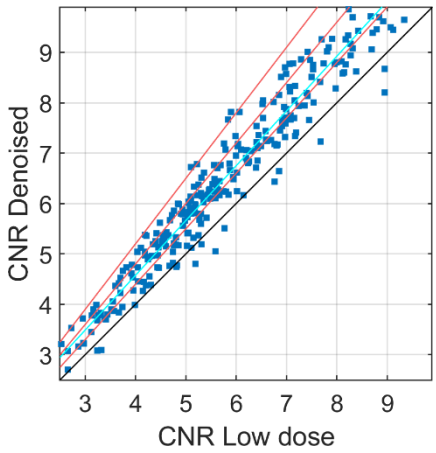

Figure 4. The CNR scatter plot of MCs from the human subjects. The cyan line indicates least squares fitting. The black line is the diagonal line. The red lines are reference lines indicating 10%, 20% and 30% gain.

4. DISCUSSION AND CONCLUSION

In this work, we proposed to denoise PVs using a DCNN before reconstruction in DBT. We designed the loss function for DCNN training and fine-tuned a pretrained CT image denoiser using DBT images of our target task. The effectiveness was shown qualitatively by visual inspection of the MC clusters and quantitatively by CNR comparisons. We showed that training with phantom images can translate to improvement in human subject images, which provides the flexibility of generating many low dose/high dose pairs for further training without the constraint of patient dose.

One advantage of denoising PVs before reconstruction is its tolerance of false-positive signals. Because our DCNN has a feature of enhancing MCs, it is possible that the DCNN treats some noise blobs as MCs and creates some false-positive signals. If the back projections of these noise blobs do not overlap during reconstruction, then the false-positive signals in the final reconstructed image will be weaker than the true-positive signals, therefore not significantly affecting MC detection.

Currently we only had a small set of paired low dose/high dose MC patches for training, and their dose difference was only a factor of two. We plan to collect a larger data set with a wider dose range for DCNN training and investigate the effect of the dose factor on training the DCNN. Further work is also needed to investigate other loss functions to balance the trade-off between noise reduction and signal preservation as well as to study the impact of PV denoising on MC detection in the reconstructed DBT by human or computer vision.

ACKNOWLEDGEMENTS

This work is supported by the National Institutes of Health under Award Number R01 CA214981.

REFERENCES

[1] J. Zheng, J. A. Fessler, and H.-P. Chan, "Detector Blur and Correlated Noise Modeling for Digital Breast Tomosynthesis Reconstruction," *IEEE Transactions on Medical Imaging*, vol. 37, no. 1, pp. 116–127, Jan. 2018, DOI: 10.1109/TMI.2017.2732824.

[2] J. Liu, A. Zarshenas, Z. Wei, L. Yang, L. Fajardo, K. Suzuki, and A. Qadir, "Radiation Dose Reduction in Digital Breast Tomosynthesis (DBT) by Means of Deep-Learning-Based Supervised Image Processing," *Proceedings of SPIE*, vol. 10574, 105740F, Mar. 2018, DOI: 10.1117/12.2293125.

[3] C. Ledig, L. Theis, F. Huszar, J. Caballero, A. Cunningham, A. Acosta, A. Aitken, A. Tejani, J. Totz, Z. Wang, and W. Shi, "Photo-Realistic Single Image Super-Resolution Using a Generative Adversarial Network," in *IEEE Conference on Computer Vision and Pattern Recognition*, 2017, pp. 105–114, DOI: 10.1109/CVPR.2017.19.

[4] K. Zhang, W. Zuo, Y. Chen, D. Meng, and L. Zhang, "Beyond a Gaussian Denoiser: Residual Learning of Deep CNN for Image Denoising," *IEEE Transactions on Image Processing*, vol. 26, no. 7, pp. 3142–3155, Jul. 2017, DOI: 10.1109/TIP.2017.2662206.

[5] H. Shan, A. Padole, F. Homayounieh, U. Kruger, R. D. Khera, C. Nitiwarangkul, M. K. Kalra, and G. Wang, "Competitive Performance of a Modularized Deep Neural Network Compared to Commercial Algorithms for Low-Dose CT Image Reconstruction," *Nature Machine Intelligence*, vol. 1, no. 6, pp. 269–276, 2019, DOI: 10.1038/s42256-019-0057-9.

[6] H.-P. Chan, M. M. Goodsitt, M. A. Helvie, S. Zelakiewicz, A. Schmitz, M. Noroozian, C. Paramagul, M. A. Roubidoux, A. V. Nees, C. H. Neal, P. Carson, Y. Lu, L. Hadjiiski, and J. Wei, "Digital Breast Tomosynthesis: Observer Performance of Clustered Microcalcification Detection on Breast Phantom Images Acquired with an Experimental System Using Variable Scan Angles, Angular Increments, and Number of Projection Views," *Radiology*, vol. 273, no. 3, pp. 675–685, 2014, DOI: 10.1148/radiol.14132722.

[7] J. Johnson, A. Alahi, and L. Fei-Fei, "Perceptual Losses for Real-Time Style Transfer and Super-Resolution," in *European Conference on Computer Vision*, 2016, pp. 694–711, DOI: 10.1007/978-3-319-46475-6_43.

[8] K. Simonyan and A. Zisserman, "Very Deep Convolutional Networks for Large-Scale Image Recognition," 04-Sep-2014. [Online]. Available: http://arxiv.org/abs/1409.1556.

[9] I. Gulrajani, F. Ahmed, M. Arjovsky, V. Dumoulin, and A. Courville, "Improved Training of Wasserstein GANs," 31-Mar-2017. [Online]. Available: http://arxiv.org/abs/1704.00028.

[10] B. Sahiner, H.-P. Chan, L. M. Hadjiiski, M. A. Helvie, J. Wei, C. Zhou, and Y. Lu, "Computer-Aided Detection of Clustered Microcalcifications in Digital Breast Tomosynthesis: a 3D Approach," *Medical Physics*, vol. 39, no. 1, pp. 28–39, Dec. 2011, DOI: 10.1118/1.3662072.

[11] J. Zheng, J. A. Fessler, and H.-P. Chan, "Segmented Separable Footprint Projector for Digital Breast Tomosynthesis and its Application for Subpixel Reconstruction," *Medical physics*, vol. 44, no. 3, pp. 986–1001, Mar. 2017, DOI: 10.1002/mp.12092.